Multiply quantized and fractional skyrmions in a binary dipolar Bose-Einstein condensate under rotation

Biao Dong,[1,2,3] Qing Sun,[4] Wu-Ming Liu,[2,3,*] An-Chun Ji,[4] Xiao-Fei Zhang,[1,3,†] and Shou-Gang Zhang[1,3,‡]
[1]*Key Laboratory of Time and Frequency Primary Standards, Chinese Academy of Sciences, Xi'an 710600, China*
[2]*Beijing National Laboratory for Condensed Matter Physics, Institute of Physics, Chinese Academy of Sciences, Beijing 100190, China*
[3]*University of Chinese Academy of Sciences, Beijing 100049, China*
[4]*Department of Physics, Capital Normal University, Beijing 100048, People's Republic of China*
(Received 25 April 2017; published 17 July 2017)

We consider a binary dipolar Bose-Einstein condensate with repulsive contact and dipolar interactions under rotation. Our results show that the interplay among short-range interaction, long-range interaction, and rotation can give rise to a rich variety of topological configurations, including giant skyrmions with multiply topological charges and skyrmion-vortex lattices. In particular, we find that for fixed rotation frequencies, tuning the short- and long-range interactions can derive novel ground-state phases, such as a meron pair composed of two fractional skyrmions and a skyrmion with topological charge $Q = 2$ centered in giant skyrmions.

DOI: 10.1103/PhysRevA.96.013619

I. INTRODUCTION

Topological defects, known as nontrivial solutions of physical systems characterized by homotopy groups under symmetry-breaking phase transitions, play central roles in many fundamental phenomena and have attracted intensive study during the past decades, ranging from condensed matter to high-energy physics [1–3]. Some kinds of topological defects, such as vortices [4], skyrmions [5,6], and merons [7,8], have been predicted or observed in condensed matter systems. In the case of spinor condensates, the competition between inter- and intracomponent contact interactions is found to yield even richer topological defects if the symmetry between the two components is broken [9]. Especially in recent years, theoretical studies of giant skyrmions [10–12] and skyrmion-lattice formation [13,14] in ultracold dilute trapped quantum gases have furnished two-species Bose-Einstein condensates (BECs) with many nontrivial spin textures by introducing extra degrees of freedom.

The subsequent and very recent achievement of two-dimensional (2D) spin-orbit (SO) coupling and topological bands for a ^{87}Rb degenerate gas through an optical Raman lattice opens a broad avenue in cold atoms to study SO-coupled condensates; there are, however, still many challenging tasks for experimentalists in realizing Rashba and Dresselhaus SO couplings [15,16]. Additionally, the emergence of a thermodynamically stable meron ground state is predicted recently due to the interplay of the single-particle Rashba SO coupling and the internal SO coupling of the dipolar interaction [17]. In contrast to the skyrmion matter dominated by SO couplings, the skyrmions in a dipolar BEC are expected to exhibit novel properties and rich phenomena [18–20], which have been ascribed to the effect of the long-range and anisotropic character of dipole-dipole interaction (DDI) in experimentally accessible quantum gases [21–25]. The long-range and anisotropic DDI has the Legendre polynomial of second order $P_2(\cos\theta)$, i.e., d-wave angular symmetry, and thus is predicted to induce novel ground-state properties and various fascinating phenomena [18,26–33]. Our previous work has shown that the inclusion of DDI introduces a "switch," which can be used not only to obtain the desired ground-state phase, but also to control the defect structures [34].

To further investigate novel features of meron pairs [8,35,36] and giant skyrmions [37,38] caused by DDI, here we consider a rotational pseudospin-1/2 system with both contact and dipolar interactions, as may result from highly magnetic (or electric) atoms such as BECs in ^{52}Cr, ^{164}Dy, or ^{168}Er [25,39–42]. Different from the system in Ref. [10], the populations of the two species in our system are equal, and the interspecies scattering length may be smaller than, equal to, or larger than the intraspecies length. Most importantly, we introduce the extra degree of freedom, namely, the anisotropic DDI, which may play a dominant role in inducing the exotic spin textures. On one hand, repulsive contact interaction between different components leads to phase separation of the two gases [43]. On the other hand, dipolar interaction breaks the rotational symmetry of the Hamiltonian in the hyperfine spin space, thus reconstructing the atomic spins and resulting in new quantum phases and topological spin textures in spinor condensates [44]. The competition between short- and long-range interactions gives rise to a spin helix [18,45,46] [see Fig. 1(c)]. As a consequence, these two kinds of interactions, together with rotation, excite substantially distinct defects, such as multiply quantized and fractional skyrmions. Employing a mean-field treatment, we explore a wealth of topological defects in the harmonically trapped BECs under rotation by tuning dipole-dipole and intercomponent interactions.

II. FORMALISM

Let us consider a cloud of two-component atomic Boson gases in which the atoms of the first component have DDI (see Fig. 1), the Hamiltonian of the system can be written as $\hat{\mathcal{H}} = \hat{\mathcal{H}}_s + \hat{\mathcal{H}}_{\text{int}}$, with

$$\hat{\mathcal{H}}_s = \left[\frac{\hat{\mathbf{p}}^2}{2m} + V(\mathbf{r}) - \Omega\hat{L}_z\right]\check{\mathrm{I}} \tag{1}$$

*wliu@iphy.ac.cn
†xfzhang@ntsc.ac.cn
‡szhang@ntsc.ac.cn

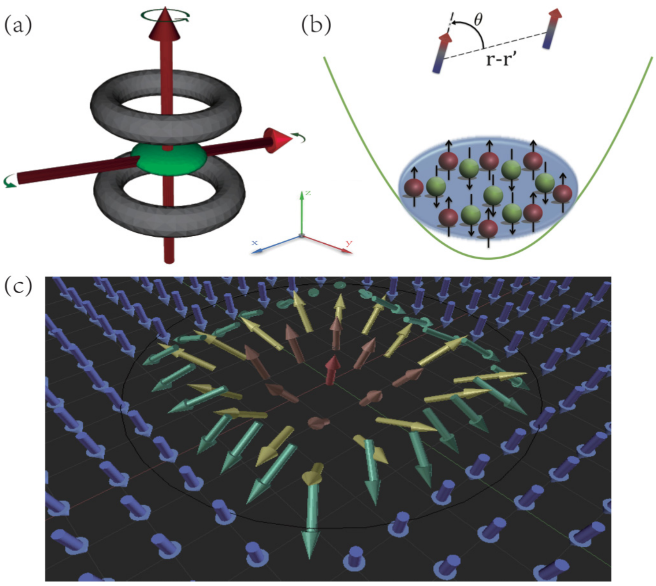

FIG. 1. (a) Atoms of the first component have magnetic dipole moments. The trapping geometry is realized by the crossed optical dipole trap (red areas) [24], and the quasi-2D BEC (green disk) is rotated with the trap beam in the $z = 0$ plane. (b) Mixture of dipolar (red spheres) and nondipolar (green spheres) atoms in a harmonic trap. Black arrows across the balls describe the pseudospin states $|\uparrow\rangle$ and $|\downarrow\rangle$. Top: Polarized atoms interact via dipole-dipole interaction separated by a distance $|\mathbf{r}-\mathbf{r}'|$, and the angle between the direction of polarization and the relative position of atoms is θ. (c) A skyrmion configuration is induced in the effective magnetic field which is generated by DDI in (a) [17].

and

$$\hat{\mathcal{H}}_{\rm int} = \hat{\mathcal{H}}_\delta + \hat{\mathcal{H}}_{\rm dd} \tag{2}$$

denoting the single-particle and interaction Hamiltonians, respectively. Here, $\hat{\mathcal{H}}_\delta$ and $\hat{\mathcal{H}}_{\rm dd}$ denote the s-wave contact and dipole-dipole interactions between atoms, $V(\mathbf{r}) = m(\omega_\perp^2 r_\perp^2 + \omega_z^2 z^2)/2$ is the external trap, $\hat{L}_z = -i\hbar(x\partial_y - y\partial_x)$ is the z component of the orbital angular momentum operator, and $\check{\mathrm{I}}$ is a 2×2 unit matrix. We assume $\omega_z \gg \omega_\perp$ for leaving the system essentially 2D in a pancake-shaped trap [see Fig. 1(a)]. By positing the separable ansatz of the wave function $\Psi(\mathbf{r}_\perp,z) = \psi(\mathbf{r}_\perp)f(z)$, the condensate is "frozen" into the ground state $f(z)$ [30].

We implement the mean-field approximation for dilute bosons at ultracold temperatures, and the ground state of the condensate is well described by the two-component $\mathbb{C}$-valued order parameter $\psi = (\psi_1,\psi_2)^T$, satisfying the normalization condition $\int |\psi_1|^2 d\mathbf{r}_\perp = \int |\psi_2|^2 d\mathbf{r}_\perp = 1$. One can derive the dimensionless nonlinear Schrödinger equation for the 2D system

$$i\frac{\partial\psi}{\partial t} = \hat{\mathcal{H}}_s'\psi + \hat{\mathcal{H}}_{\rm int}'\psi, \tag{3}$$

where the dimensionless single-particle Hamiltonian

$$\hat{\mathcal{H}}_s' = \left\{-\tfrac{1}{2}\nabla^2 + \tfrac{1}{2}(x^2+y^2) - \Omega[-i(x\partial_y - y\partial_x)]\right\}\check{\mathrm{I}}. \tag{4}$$

Here, we work in characteristic units by scaling with the trap energy $\hbar\omega_z$ and the axial harmonic oscillator length $l_z = \sqrt{\hbar/m\omega_z}$. The dimensionless nonlinear interaction term is

$$\hat{\mathcal{H}}_{\rm int}' = \hat{U} + \hat{\Phi}_{\rm dd} = \begin{pmatrix} U_1 + \Phi_{\rm dd}^1 & 0 \\ 0 & U_2 + \Phi_{\rm dd}^2 \end{pmatrix}, \tag{5}$$

where the contact interactions $U_{i=1,2} = \sum_{j=1,2} g_{ij}\rho_j$ with intra- and interspecies coupling strengths $g_{ii} = 2\sqrt{2\pi}a_{ii}$ and $g_{ij} = 2\sqrt{2\pi}a_{ij}$, respectively, where a_{ij} are the corresponding s-wave scattering lengths. The density of the ith component is $\rho_i(\mathbf{r}_\perp,t) = |\psi_i(\mathbf{r}_\perp,t)|^2$, and the dipolar interactions $\Phi_{\rm dd}^i(\mathbf{r}_\perp,t) = \sum_{j=1,2}\int U_{\rm dd}^{ij}(\mathbf{r}_\perp - \mathbf{r}'_\perp)\rho_i(\mathbf{r}'_\perp,t)d\mathbf{r}'_\perp$. When all dipoles are polarized along the same direction by an external field, the explicit dipole-dipole interactions read [18]

$$U_{\rm dd}^{ij}(\mathbf{r}_\perp - \mathbf{r}'_\perp) = \frac{C_{\rm dd}^{ij}}{4\pi}\frac{1-3\cos^2\theta}{|\,\mathbf{r}_\perp - \mathbf{r}'_\perp\,|^3}, \tag{6}$$

where $C_{\rm dd} = \mu_0\mu^2$, with μ being the magnetic dipole moment and μ_0 the vacuum permeability. θ is the angle between the direction of polarization and the relative position of atoms [see Fig. 1(b)]. We assume that $C_{\rm dd}^{22} = C_{\rm dd}^{12} = C_{\rm dd}^{21} = 0$, i.e., only the first component has dipolar interaction. Note that in the absence of an external magnetic field, the Hamiltonian of the spinor BEC is rotationally invariant in the hyperfine spin space; the anisotropic DDI breaks this symmetry, inducing novel quantum phases by tuning the effective strength of DDI via a modification of the trapping geometry or the relative strength of usual isotropic contact interaction by Feshbach resonance [18,23–25] (see Fig. 1).

To obtain the ground-state wave function ψ, it is convenient to write the Gross-Pitaevskii energy

$$\mathcal{E}[\psi^*,\psi] = \int d^2\mathbf{r}\left\{\psi^*\left(-\frac{\nabla^2}{2} + \frac{r_\perp^2}{2} - \Omega\hat{L}_z'\right)\check{\mathrm{I}}\psi + \frac{1}{2}\psi^*\hat{\Phi}_{\rm dd}\psi + \frac{g_{11}+g_{12}}{2}|\psi^*\psi|^2 + \frac{g_{11}-g_{12}}{2}|\psi^*\hat{\sigma}_z\psi|^2\right\}, \tag{7}$$

where $\hat{L}_z' = -i(x\partial_y - y\partial_x)$ is the dimensionless orbital angular momentum and $\hat{\sigma}_z$ is the z component of the 2×2 Pauli matrix.

III. RESULTS AND DISCUSSION

By numerically minimizing the energy function $\mathcal{E}[\psi^*,\psi]$ in Eq. (7), we can obtain the ground states of the dipolar BECs in a harmonic trap under rotation [47]. In general, once a condensate is rotated, topological defects, such as quantized vortices [4,48], skyrmions [49], and merons [8], will be excited. And more defects would be formed by increasing the angular momentum or introducing repulsive DDI. To guide the analysis, we fix the contact interactions $g = g_{11} = g_{22} = 100$ and investigate distinct ground states by varying the ratio between inter- and intrainteractions $\gamma = g_{12}/g$.

A. Giant skyrmion phase

To study the competition between contact and dipolar interactions, we first consider a binary BEC without DDI and then polarize the dipoles along a fixed angle to find

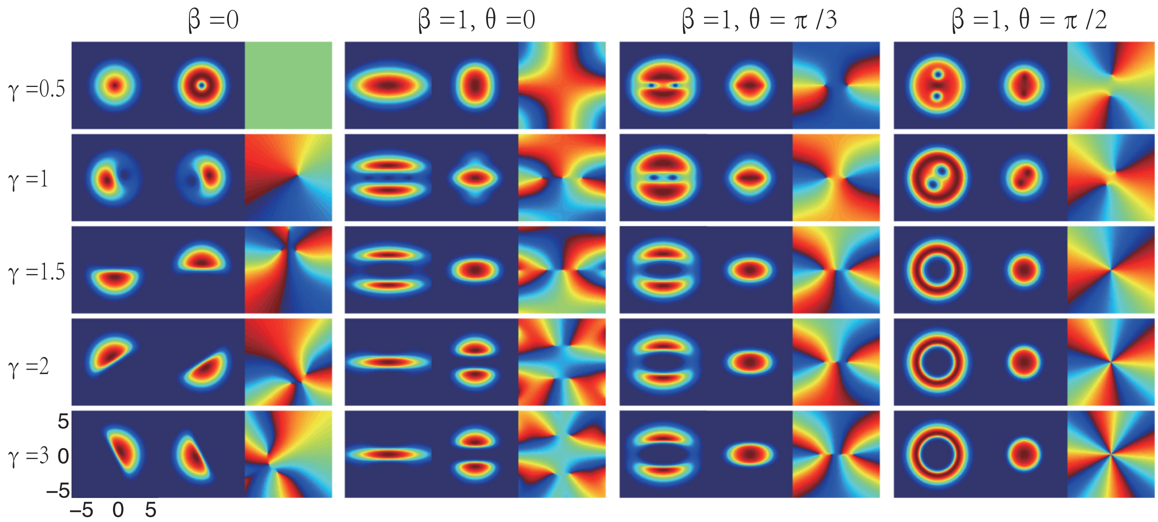

FIG. 2. Ground-state density and phase distributions of the two components for varied inter-component and dipole-dipole interactions under the rotation frequency $\Omega = 0.3$. From left to right in each column: density $\rho_1 = |\psi_1|^2$, density $\rho_2 = |\psi_2|^2$, and phase $\phi_1 = \arg\psi_1$. The density is indicated by a color map from red (high) to blue (low), and the phase ranges from $-\pi$ (blue) to π (red). β is the ratio between dipolar and intracomponent contact interactions, γ is the ratio between inter- and intracomponent interactions, and θ is the angle between the direction of polarization and the relative position of atoms.

the effect of the anisotropic DDI. In the absence of DDI, the repulsive interaction between the two species breaks the rotational symmetry of the Hamiltonian in real space. As a result, atoms in the two components feel repulsion for each other and occupy the location of a random direction in real space. The left column in Fig. 2 shows the phase separation of the two-component BEC, from whose phase profiles we can distinguish that due to the rotation; the hidden quantized vortices [50–52] are excited near the separated lines of the two disks. However, in the presence of DDI, the contact interaction competes with the DDI in the first component, resulting in novel density distributions. To highlight the effect of DDI, we consider three cases in the following discussion. Here, the ratio between dipolar and intracomponent contact interactions is $\beta = \frac{4\pi}{3}\frac{g_d}{g} = \frac{\sqrt{8\pi}C_{\mathrm{dd}}}{3g} = 1$. When the orientation of the dipoles is aligned along the x-axis direction ($\theta = 0$, as shown in the second column in Fig. 2), we observe stripe patterns of vortices due to the anisotropy of the DDIs, which are attractive in the x-axis direction but repulsive in the y-axis direction [20]. When the orientation of the dipoles is aligned along a tilting direction from the 2D plane (e.g., $\theta = \pi/3$, as shown in the third column in Fig. 2), attraction on the x axis is weakened and repulsion of the dipolar condensate dominates the atoms. Thus, the cloud of the dipolar condensate prefers to locate in the periphery, and the scalar (second-component) cloud is contracted in the y-axis direction as the repulsive interspecies interaction γ becomes stronger. When the orientation of the dipoles is aligned along the z axis ($\theta = \pi/2$, as shown in the rightmost column in Fig. 2), "purely" repulsive interaction of the dipoles in the first component causes spreading of the condensate spreading occupy the outside area. Contrarily, the scalar BEC locates in the inside area in the presence of repulsive contact interaction between two condensates. When the repulsive intercomponent interaction is increased to $\gamma > 1$, contact interaction dominates in the system and leads to phase separation between the two disks as a centrosymmetric structure. Meanwhile, defects in the dipolar condensate induced by the rotation conjoin as the enlargement of γ to form a giant hole. Thus, the atoms in the first component occupy the periphery and take a toroidal-shaped formation in the dipolar disk, while the scalar condensate fills the giant hole. As a consequence, the *giant skyrmions* shown in the rightmost column in Fig. 2 exist owing to the competition of short- and long-range interactions. Moreover, the topological charge of the giant skyrmion which is *doubly* quantized rises to *triply* and then to *quadruply* quantized when the intercomponent interaction is continuously increased (as shown in the rightmost column in Fig. 2).

B. Fractional skyrmion phase

For the reason of the stability of a dipolar BEC in a pancake-shaped trap [24], in the following discussion we fix the polarization axis of the dipoles paralleled with the z axis ($\theta = \pi/2$; in this case the dipoles repel each other and the BEC is stable [24]) and investigate the topological phases under the effect of DDI with a stronger rotation frequency (see Fig. 3). Obviously, more vortices are generated to form vortex "necklaces" when we augment the rotation speed to $\Omega = 0.5$ and 0.6 for $\gamma < \gamma_{c1}$ (e.g., $\gamma_{c1} = 0.85$ for $\Omega = 0.6$). However, when we increase the intercomponent interactions above some critical values ($\gamma \geq \gamma_{c1}$), these vortices unite to become a giant skyrmion, because the repulsive interaction between dipolar and nondipolar gases exerts force on them, separating them into immiscible condensates. An isolated (or triangular-lattice) skyrmion is also induced in the scalar condensate owing to the strong rotation frequency for $\Omega = 0.5$ (or 0.6). As the repulsion is increased further, the atoms in the second component will be repelled farther by the first component, and thus the radius of the skyrmion in the scalar condensate will decrease. Correspondingly, the density peak(s) in the center of the dipolar condensate repels the atoms from the scalar one and gradually forms an isolated peak as repulsive

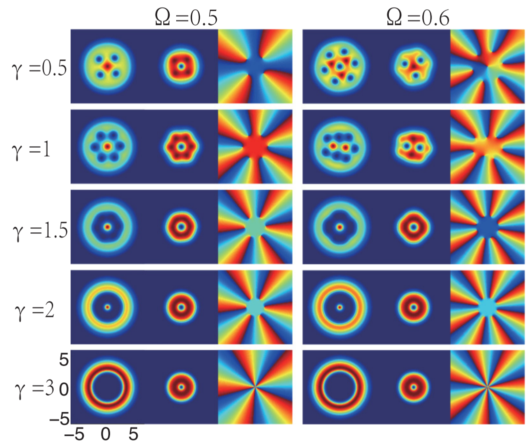

FIG. 3. Vortex necklaces conjoin with giant skyrmions in rotating BECs as intercomponent interactions γ are increased. The color map and parameters are the same as in the rightmost column in Fig. 2, but for the rotation frequency $\Omega = 0.5$ (left column) and $\Omega = 0.6$ (right column). Meron pairs emerge when $\gamma \sim 1$ for $\Omega = 0.6$, and the topological charge of a meron for $\gamma \in [0.85, 1.3)$ is $Q = \frac{1}{2}$.

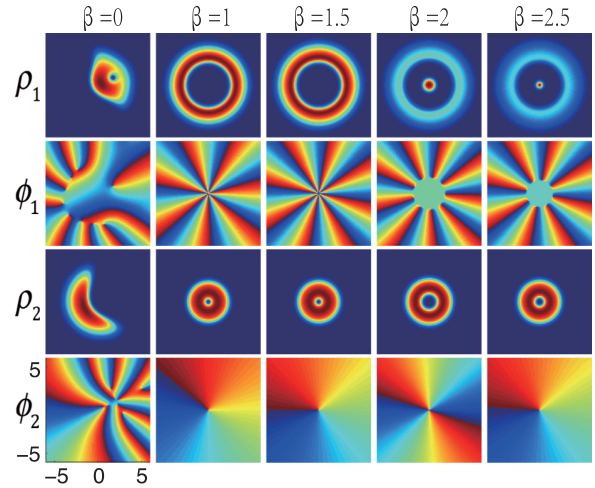

FIG. 4. Density and phase profiles of giant skyrmions with different quantized numbers in a dipolar BEC. A doubly quantized skyrmion ($Q = 2$) is formed in the center when $\beta = 2$. Here the parameters are chosen as $\Omega = 0.6$ and $\gamma = 3$. Color map same as for Fig. 2.

contact interaction (γ) increases. In the following descriptions, we show that these peaks may have fractionally or doubly quantized topological charges. Feeling a larger repulsion from the scalar condensate (see the right column in Fig. 3), peaks in the dipolar disk or skyrmions in the scalar disk reconstruct and induce a *meron pair* near the center of the condensate when we increase the intercomponent interaction to $\gamma_{c1} \leq \gamma < \gamma_{c2}$ $(0.85 \leq \gamma < 1.3)$, and the two merons finally conjoin to a skyrmion as $\gamma \geq 1.3$. Finally, the narrow peak is shoved to the outer large torus by the stronger contact repulsion and vanishes (see the lowest two panels in Fig. 3 when $\gamma = 3$).

The spins in a giant skyrmion may twist from up at the center to all down at the boundary, which is different from the case of a giant vortex [10,37,53]. In contrast to the topological point defect of a vortex characterized by the quantized winding number, a skyrmion [a type of magnetic vortex [6]; Fig. 1(c)] is a topological spin texture characterized by the quantized *topological charge*—the skyrmion number—defined by [19,53–58]

$$Q = \frac{1}{4\pi} \int d^2\mathbf{r} \hat{\mathbf{M}} \cdot \frac{\partial \hat{\mathbf{M}}}{\partial x} \times \frac{\partial \hat{\mathbf{M}}}{\partial y}, \tag{8}$$

where $\hat{\mathbf{M}} = \psi^\dagger(\frac{1}{2}\sigma)\psi/\psi^\dagger\psi$ is the unit vector of the local magnetization and the integral is taken over a 2D unit cell. A meron is a topological defect with fractional topological charge $Q = 1/2$. It is a nonlocal object whose action happens to diverge logarithmically as $\sim 1/\tilde{g}^2 \ln R$, where $\tilde{g}$ is the quantum chromodynamics coupling constant and R the radius of Euclidean space [3,19,59,60]. However, a meron and antimeron pairing bound state with $Q = 1$ has finite action with finite separation R.

C. Doubly quantized skyrmion and skyrmion-vortex lattice phases

As stated before, the anisotropic DDI can break the rotational symmetry of the Hamiltonian in the hyperfine spin space and induce novel quantum phases. Figures 4 and 5 clearly reveal the competition between short- and long-range interactions. In the absence of DDI, topological (hidden) defects are induced by rotation, and phase separation in a random direction will be observed due to the broken rotational symmetry of the two condensates from repulsive contact interaction, as shown in the first column in Fig. 4. The topological charge of the giant skyrmion becomes larger as the DDI is increased between $1 \leq \beta \leq 2$ when $\Omega = 0.6$ as shown in the second, third, and fourth columns in Fig. 4. Intriguingly, a skyrmion with topological charge $Q = 2$ (see the fourth column in Fig. 4), or a *doubly quantized skyrmion*, is centered in a giant skyrmion when β is augmented over a critical one β_{c1} ($\lesssim$2). It is a tightly bound state of two skyrmions with opposite helicities and has been generated in an anisotropic frustrated

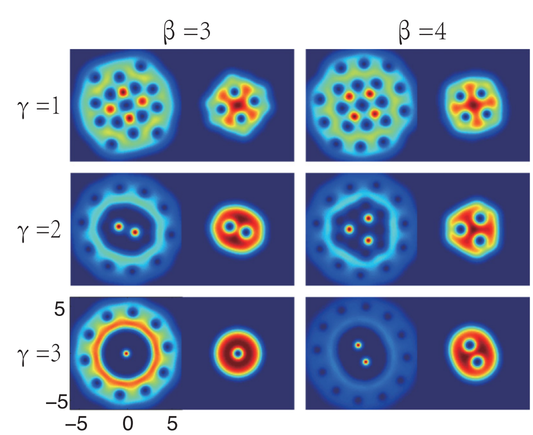

FIG. 5. Ground-state density distributions of skyrmion-vortex lattices ($\gamma = 1, \beta = 3$ or 4), an isolate skyrmion rounded by a vortex ring ($\gamma = 3, \beta = 3$), skyrmion pairs rounded by vortex rings ($\gamma = 2$, $\beta = 3$ or $\gamma = 3, \beta = 4$), and triangular-type skyrmions rounded by a vortex ring ($\gamma = 2, \beta = 4$). The rotation frequency is fixed at $\Omega = 0.7$. Color map of the density same as for Fig. 2.

(or inversion-symmetric) magnet [46,61]. In our situation of a dipolar BEC, it comes from the effect of a strong DDI, which can reconstruct the density distribution and induce a totally novel spin configuration. Actually, as shown in the fourth column in Fig. 4, the small peak in the center of the dipolar component results from strongly repulsive dipoles of the giant torus. The strong repulsion in the peak competes over the shove from the scalar condensate and broadens the radius of the hole in another component to form a doubly quantized skyrmion. However, the radius of the skyrmion in the center decreases quickly when the strength of DDI is further increased over a second critical value β_{c2} ($\lesssim$2.5), and the skyrmion again becomes a single one (see the rightmost column in Fig. 4). That is, repulsive DDIs in the peak of the dipolar disk are strong enough to extrude the atoms from the center to the outside giant torus, so that the doubly quantized skyrmion only exists within $\beta_{c1} < \beta < \beta_{c2}$, which is a balanced region between repulsive dipoles and intercomponent interaction. It is an obvious effect of the competition between repulsive contact and dipolar interactions. Some exotic phases, such as skyrmion-vortex lattices and paired- and triangular-type skymions rounded by vortex rings, also emerge in the BECs due to the competitions of contact and dipolar interactions under strong rotation frequencies, as shown in Fig. 5. On one hand, more vortices in the giant torus with more skyrmions in the center will be induced as β increases. On the other hand, increasing γ reduces the number of skymions in the center. As a consequence, different phases exist in each balanced parameter region owing to the competitions of the repulsive interactions between atoms.

D. Spin textures

To understand the topological structures of the skyrmion ground states, we obtain rotationally symmetric spin textures in Fig. 6. Figures 6(a1)–6(d1) show the geometric variability of the texture in a giant skyrmion which is conjoint from two skyrmions [Fig. 6(a1)] in a weakly rotating BEC ($\Omega = 0.3$; see the rightmost column in Fig. 2). As the topological charge rises from 2 to 4, the triangular-shaped giant torus with spins twisting around it [Fig. 6(b1)] becomes cubic and pentagon shaped [Figs. 6(c1) and 6(d1)]. Figures 6(a2)–6(d2) show the spin textures of giant skyrmions which are conjoint from triangular-lattice skyrmions [Fig. 6(a2)] in a strongly rotating BEC ($\Omega = 0.6$; see the rightmost column in Fig. 3). Figures 6(b2) and 6(c2) show the central twists rounded by giant topological tori with total topological charge $Q = 8$. As shown in Fig. 3, the central peak of the dipolar condensate may vanish due to stronger repulsion from the scalar condensate. Correspondingly, the topological structure of central spin texture shown in Fig. 6(c2) vanishes as well and becomes that shown in Fig. 6(d2), with the total topological charge decreasing to $Q = 6$. Thus, we can draw the conclusion that the topological skyrmion structure of the central peak in the condensate comes from the competition of repulsive short- and long-range interactions under strong rotation. In addition, under rotation frequency $\Omega = 0.7$, richer topological spin textures, such as skyrmion-vortex lattices [Figs. 6(a3) and 6(b3)], also emerge when a stronger DDI dominates in the system. As the intercomponent interaction is increased to

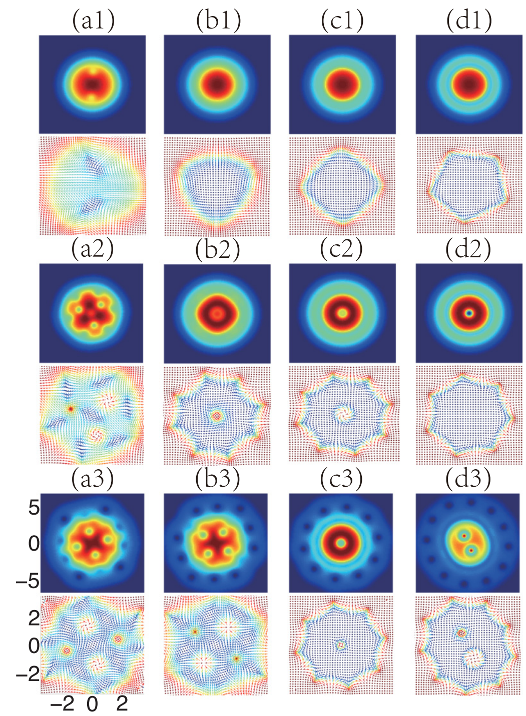

FIG. 6. Topological and rotationally symmetric ground-state structures of the total density profiles $\rho = |\psi_1|^2 + |\psi_2|^2$ and their corresponding spin textures. Color map of the density same as for Fig. 2. Values of the pseudospin density are from −1 (blue) to 1 (red). The parameters (Ω,β,γ) are chosen as (a1) (0.3,1,0.5), (b1) (0.3,1,1.5), (c1) (0.3,1,2), (d1) (0.3,1,3), (a2) (0.6,1,0.5), (b2) (0.6,1,1.5), (c2) (0.6,1,2), (d2) (0.6,1,3), (a3) (0.7,3,1), (b3) (0.7,4,1), (c3) (0.7,3,3), and (d3) (0.7,4,3), respectively.

$\gamma = 3$, an isolated skyrmion and a pair of skyrmions with (anti-)clockwise rotating vorticity rounded by vortex rings [Figs. 6(c3) and 6(d3)] are observed when DDI is $\beta = 3$ and 4, respectively.

Figure 7 shows the spin textures of different types of skyrmions with different topological charges. Figure 7(a) presents a typical spin texture for a skyrmion with $Q = 1$ [in which the spins at the center point out of the page and those at the edge point into the page on a 2D plane as shown in Fig. 1(c)], centered in a giant skymion. It corresponds to the distribution shown in the left column in Fig. 3 when the parameters are chosen as $\Omega = 0.5$, $\beta = 1$, and $\gamma = 2$. In one case, this skyrmion may split into two fractional skyrmions, called a meron pair, with (anti-)clockwise rotating vorticity, whose topological charge is $Q = 1/2$, as shown in Fig. 7(b). This phenomenon, resulting from the balanced condition $\gamma_{c1} \leq \gamma < \gamma_{c2}$ $(0.85 \leq \gamma < 1.3)$ when the intercomponent interaction is comparable to the DDI, emerges under strong rotation (e.g., $\Omega = 0.6$), which is shown in the right column in Fig. 3 as we have discussed before. In another case, two skyrmions may mix together to form a doubly quantized skyrmion [$Q = 2$; Fig. 7(c)], in which the planar projection of the spins rotates twice as one circles the origin [62]. It is a situation under the balanced condition $\beta_{c1} < \beta < \beta_{c2}$ ($\beta_{c1} \lesssim 2$ and $\beta_{c2} \lesssim 2.5$) with strongly repulsive interspecies interaction $(\gamma = 3)$ under rotation frequency $\Omega = 0.6$, as

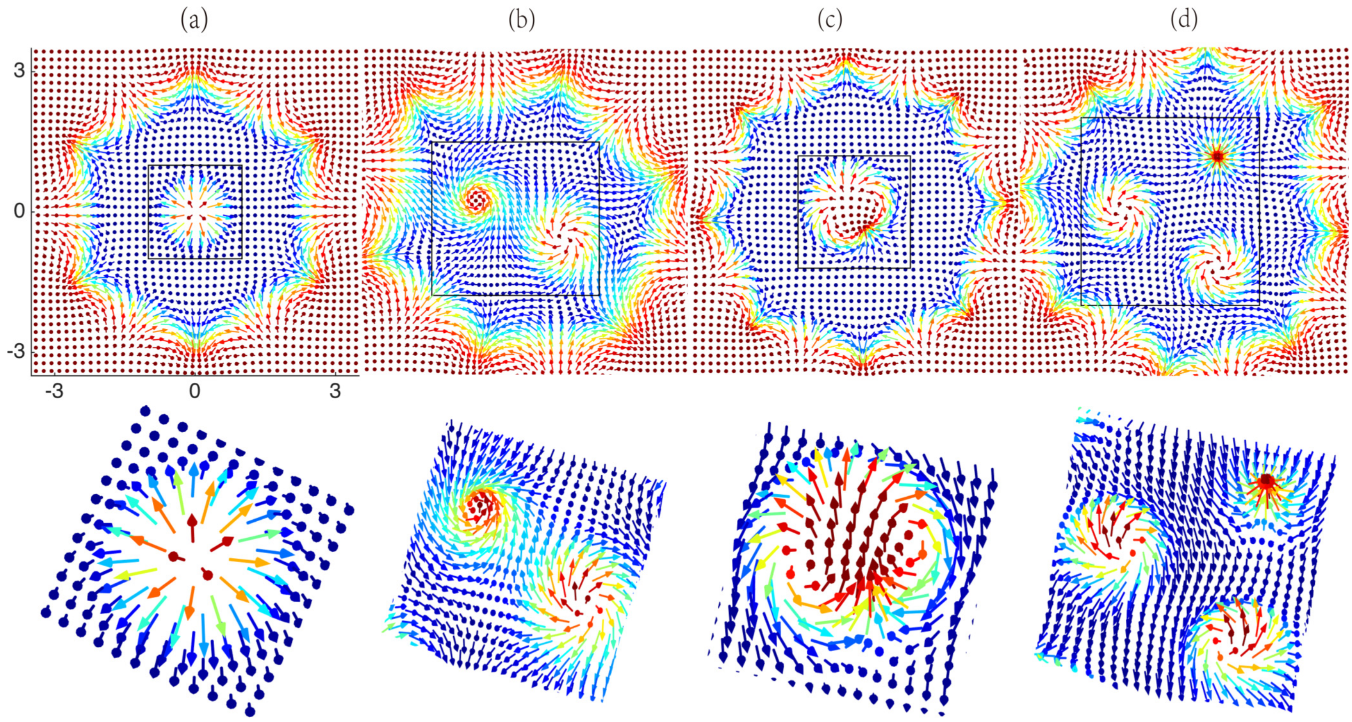

FIG. 7. Examples of spin textures of different kinds of skyrmions with different topological charges. Systems with the same parameters as in the left column in Fig. 3 ($\Omega = 0.5$, $\beta = 1$, $\gamma = 2$), the right column in Fig. 3 ($\Omega = 0.6$, $\beta = 1$, $\gamma = 1.29$), the fourth column in Fig. 4 ($\Omega = 0.6$, $\beta = 2$, $\gamma = 3$), and the right column in Fig. 5 ($\Omega = 0.7$, $\beta = 4$, $\gamma = 2$). Lower panels are zoom-ins of the regions in the rectangles the upper panels. Values of the pseudospin density are from -1 (blue) to 1 (red).

shown in the fourth column in Fig. 4. Owing to the competition, three skyrmions, constituting a triangular-type structure with different kinds of vorticities, are also observed, as shown in Fig. 7(d), when we increase both the rotation frequency and the dipole-dipole interaction further (corresponding to the middle panel, right column, in Fig. 5, where the parameters are $\Omega = 0.7$, $\gamma = 2$, and $\beta = 4$).

We now give an experimental protocol for observing the above exotic states in future experiments. This specific system can be realized by selecting two states in the ground hyperfine manifolds of atomic Cr, Er, or Dy, where components 1 and 2 can consist of states with spin projections $m_J = -J$ and $m_J = 0$ [23,63]. The condensate can be reached by cooling 3×10^4 atoms in a harmonic trap with frequency $\omega_\perp = 2\pi \times 300$ Hz, and the strongly dipolar regime $\beta = \mu_0\mu^2 m/3\hbar^2 a_s > 1$ can be realized by employing Feshbach resonance through reduction of the intercomponent scattering length [34,39,52]. Using an off-resonant laser beam to provide a rotating gradient [64], a BEC can be stirred and possess an angular momentum with a frequency exceeding $\Omega = 0.8\omega_\perp$ [65], thus the system can be coupled by the laser beam when choosing $\Omega = (0.3,0.5,0.6,0.7) \times \omega_\perp = 2\pi \times (90,150,180,210)$ Hz. Consequently, we conclude that the parameters used in this paper are within the current experimental capacity.

IV. CONCLUSIONS

In summary, we have investigated the ground-state properties of a binary dipolar BEC under rotation. Our results show the competition among rotation, contact, and dipolar interactions leading to the formation of various topological structures, such as giant skyrmions, skyrmion-vortex lattices, and paired- and triangular-type skymions rounded by vortex rings. Compared to the previous binary condensate without dipole-dipole interaction, we first observe a meron pair formed by two fractional skyrmions and a doubly quantized skyrmion centered in giant skyrmions in the case of strong rotation. Meron pairs are observed under the balanced condition when the ratio between inter- and intracomponent interactions is $0.85 \leq \gamma < 1.3$ and the ratio between dipolar and intracomponent contact interactions $\beta = 1$. However, doubly quantized skyrmions are observed under the balanced condition $2 \lesssim \beta \lesssim 2.5$ with strongly repulsive interspecies interaction ($\gamma = 3$). Due to the high degrees of control over most of the system parameters, the various topological structures studied in this paper are within the reach of current experiments with ultracold atoms.

ACKNOWLEDGMENTS

B.D. thanks R. M. Wilson, S. Yi, and W. Han for helpful discussions. This work was supported by the NKRDP under Grant No. 2016YFA0301500; the NSFC under Grants No. 11434015, No. 61227902, No. 61378017, No. 11303030, No. 91336101, No. 11474282, and No. KZ201610005011; the SKLQOQOD under Grant No. KF201403; and the SPRPCAS under Grants No. XDB01020300 and No. XDB21030300. X.-F.Z. is also supported by the Youth Innovation Promotion Association of CAS under Grant No. 2015334.

[1] N. D. Mermin, Rev. Mod. Phys. **51**, 591 (1979).
[2] A. Vilenkin and E. P. S. Shellard, *Cosmic Strings and other Topological Defects* (Cambridge University Press, Cambridge, UK, 1994).
[3] H.-B. Braun, Adv. Phys. **61**, 1 (2012).
[4] A. L. Fetter, Rev. Mod. Phys. **81**, 647 (2009).
[5] U. A. Khawaja and H. Stoof, Nature (London) **411**, 918 (2001).
[6] S. Mühlbauer, B. Binz, F. Jonietz, C. Pfleiderer, A. Rosch, A. Neubauer, R. Georgii, and P. Böni, Science **323**, 915 (2009).
[7] T. Mizushima, K. Machida, and T. Kita, Phys. Rev. Lett. **89**, 030401 (2002).
[8] K. Kasamatsu, M. Tsubota, and M. Ueda, Phys. Rev. Lett. **93**, 250406 (2004).
[9] X.-Q. Xu and J. H. Han, Phys. Rev. Lett. **107**, 200401 (2011).
[10] S.-J. Yang, Q.-S. Wu, S.-N. Zhang, and S. Feng, Phys. Rev. A **77**, 033621 (2008).
[11] P. Mason and A. Aftalion, Phys. Rev. A **84**, 033611 (2011).
[12] P. Kuopanportti, N. V. Orlova, and M. V. Milošević, Phys. Rev. A **91**, 043605 (2015).
[13] H. Hu, B. Ramachandhran, H. Pu, and X.-J. Liu, Phys. Rev. Lett. **108**, 010402 (2012).
[14] Z.-F. Xu, S. Kobayashi, and M. Ueda, Phys. Rev. A **88**, 013621 (2013).
[15] Z. Wu, L. Zhang, W. Sun, X.-T. Xu, B.-Z. Wang, S.-C. Ji, Y. Deng, S. Chen, X.-J. Liu, and J.-W. Pan, Science **354**, 83 (2016).
[16] L. Huang, Z. Meng, P. Wang, P. Peng, S.-L. Zhang, L. Chen, D. Li, Q. Zhou, and J. Zhang, Nat. Phys. **12**, 540 (2016).
[17] R. M. Wilson, B. M. Anderson, and C. W. Clark, Phys. Rev. Lett. **111**, 185303 (2013).
[18] T. Lahaye, C. Menotti, L. Santos, M. Lewenstein, and T. Pfau, Rep. Prog. Phys. **72**, 126401 (2009).
[19] N. Nagaosa and Y. Tokura, Nat. Nano **8**, 899 (2013).
[20] Y. Zhao, J. An, and C.-D. Gong, Phys. Rev. A **87**, 013605 (2013).
[21] S. Yi and L. You, Phys. Rev. A **61**, 041604(R) (2000); **63**, 053607 (2001).
[22] J. Stuhler, A. Griesmaier, T. Koch, M. Fattori, T. Pfau, S. Giovanazzi, P. Pedri, and L. Santos, Phys. Rev. Lett. **95**, 150406 (2005).
[23] T. Lahaye, T. Koch, B. Fröhlich, M. Fattori, J. Metz, A. Griesmaier, S. Giovanazzi, and T. Pfau, Nature (London) **448**, 672 (2007).
[24] T. Koch, T. Lahaye, J. Metz, B. Fröhlich, A. Griesmaier, and T. Pfau, Nat. Phys. **4**, 218 (2008).
[25] M. Lu, N. Q. Burdick, S. H. Youn, and B. L. Lev, Phys. Rev. Lett. **107**, 190401 (2011).
[26] L. Santos, G. V. Shlyapnikov, and M. Lewenstein, Phys. Rev. Lett. **90**, 250403 (2003).
[27] Y. Kawaguchi, H. Saito, and M. Ueda, Phys. Rev. Lett. **96**, 080405 (2006); **97**, 130404 (2006).
[28] R. M. Wilson, S. Ronen, J. L. Bohn, and H. Pu, Phys. Rev. Lett. **100**, 245302 (2008).
[29] T. Lahaye, J. Metz, B. Fröhlich, T. Koch, M. Meister, A. Griesmaier, T. Pfau, H. Saito, Y. Kawaguchi, and M. Ueda, Phys. Rev. Lett. **101**, 080401 (2008).
[30] R. Nath, P. Pedri, and L. Santos, Phys. Rev. Lett. **102**, 050401 (2009).
[31] C. Ticknor, R. M. Wilson, and J. L. Bohn, Phys. Rev. Lett. **106**, 065301 (2011).
[32] Y. Deng, J. Cheng, H. Jing, C.-P. Sun, and S. Yi, Phys. Rev. Lett. **108**, 125301 (2012).
[33] X. Jiang, Z. Fan, Z. Chen, W. Pang, Y. Li, and B. A. Malomed, Phys. Rev. A **93**, 023633 (2016).
[34] X.-F. Zhang, L. Wen, C.-Q. Dai, R.-F. Dong, H.-F. Jiang, H. Chang, and S.-G. Zhang, Sci. Rep. **6**, 19380 (2016).
[35] X.-F. Zhang, R.-F. Dong, T. Liu, W. M. Liu, and S.-G. Zhang, Phys. Rev. A **86**, 063628 (2012).
[36] S.-Z. Lin, A. Saxena, and C. D. Batista, Phys. Rev. B **91**, 224407 (2015).
[37] M. Ezawa, Phys. Rev. Lett. **105**, 197202 (2010).
[38] A. Aftalion and P. Mason, Phys. Rev. A **88**, 023610 (2013).
[39] A. Griesmaier, J. Werner, S. Hensler, J. Stuhler, and T. Pfau, Phys. Rev. Lett. **94**, 160401 (2005).
[40] B. Pasquiou, E. Maréchal, G. Bismut, P. Pedri, L. Vernac, O. Gorceix, and B. Laburthe-Tolra, Phys. Rev. Lett. **106**, 255303 (2011).
[41] K. Aikawa, A. Frisch, M. Mark, S. Baier, A. Rietzler, R. Grimm, and F. Ferlaino, Phys. Rev. Lett. **108**, 210401 (2012).
[42] M. A. Baranov, M. Dalmonte, G. Pupillo, and P. Zoller, Chem. Rev. **112**, 5012 (2012).
[43] S. B. Papp, J. M. Pino, and C. E. Wieman, Phys. Rev. Lett. **101**, 040402 (2008).
[44] S. Yi, L. You, and H. Pu, Phys. Rev. Lett. **93**, 040403 (2004).
[45] A. Manchon, H. C. Koo, J. Nitta, S. M. Frolov, and R. A. Duine, Nat. Mater. **14**, 871 (2015).
[46] A. O. Leonov and M. Mostovoy, Nat. Commun. **6**, 8275 (2015).
[47] C. J. Pethick and H. Smith, *Bose-Einstein Condensation in Dilute Gases* (Cambridge University Press, Cambridge, UK, 2002).
[48] A.-C. Ji, W. M. Liu, J. L. Song, and F. Zhou, Phys. Rev. Lett. **101**, 010402 (2008).
[49] S.-W. Su, C.-H. Hsueh, I.-K. Liu, T.-L. Horng, Y.-C. Tsai, S.-C. Gou, and W. M. Liu, Phys. Rev. A **84**, 023601 (2011).
[50] L. Wen, H. Xiong, and B. Wu, Phys. Rev. A **82**, 053627 (2010).
[51] T. Mithun, K. Porsezian, and B. Dey, Phys. Rev. A **89**, 053625 (2014).
[52] X.-F. Zhang, W. Han, L. Wen, P. Zhang, R.-F. Dong, H. Chang, and S.-G. Zhang, Sci. Rep. **5**, 8684 (2015).
[53] S. Banerjee, J. Rowland, O. Erten, and M. Randeria, Phys. Rev. X **4**, 031045 (2014).
[54] C. M. Savage and J. Ruostekoski, Phys. Rev. Lett. **91**, 010403 (2003).
[55] X. Z. Yu, Y. Onose, N. Kanazawa, J. H. Park, J. H. Han, Y. Matsui, N. Nagaosa, and Y. Tokura, Nature (London) **465**, 901 (2010).
[56] R. W. Cherng and E. Demler, Phys. Rev. A **83**, 053614 (2011).
[57] S. Heinze, K. von Bergmann, M. Menzel, J. Brede, A. Kubetzka, R. Wiesendanger, G. Bihlmayer, and S. Blügel, Nat. Phys. **7**, 713 (2011).
[58] J. Iwasaki, M. Mochizuki, and N. Nagaosa, Nat. Nano **8**, 742 (2013).
[59] C. G. Callan, R. Dashen, and D. J. Gross, Phys. Rev. D **17**, 2717 (1978).

[60] R. Rajaraman, *Solitons and Instantons: An Introduction to Solitons and Instantons in Quantum Field Theory* (North-Holland Personal Library, Amsterdam, 1987).
[61] S.-Z. Lin and S. Hayami, Phys. Rev. B **93**, 064430 (2016).
[62] E. J. Mueller, Phys. Rev. A **69**, 033606 (2004).
[63] W. E. Shirley, B. M. Anderson, C. W. Clark, and R. M. Wilson, Phys. Rev. Lett. **113**, 165301 (2014).
[64] M. R. Matthews, B. P. Anderson, P. C. Haljan, D. S. Hall, C. E. Wieman, and E. A. Cornell, Phys. Rev. Lett. **83**, 2498 (1999).
[65] K. W. Madison, F. Chevy, W. Wohlleben, and J. Dalibard, Phys. Rev. Lett. **84**, 806 (2000).